ISSN 0915-633X

NATIONAL INSTITUTE FOR FUSION SCIENCE

Analysis of Radial Electric Field in LHD towards Improved Confinement

M. Yokoyama, K. Ida, H. Sanuki, K. Itoh, K. Narihara, K. Tanaka,
K. Kawahata, N. Ohyabu and LHD experimental group

(Received - Apr. 13, 2001)

NIFS-696 May 2001

RESEARCH REPORT
NIFS Series

TOKI, JAPAN

Analysis of Radial Electric Field in LHD towards Improved Confinement

M. YOKOYAMA, K. IDA, H. SANUKI, K. ITOH, K. NARIHARA, K. TANAKA, K. KAWAHATA, N. OHYABU and LHD EXPERIMENTAL GROUP

National Institute for Fusion Science, Toki 509-5292, Japan

The radial electric field (E_r) properties in LHD have been investigated to indicate the guidance towards improved confinement with possible E_r transition and bifurcation. The ambipolar E_r is obtained from the neoclassical flux based on the analytical formulae. This approach is appropriate to clarify ambipolar E_r properties in a wide range of temperature and density in a more transparent way. The comparison between calculated E_r and experimentally measured one has shown the qualitatively good agreement such as the threshold density for the transition from ion root to electron root. The calculations also well reproduce the experimentally obesrved tendency that the electron root is possible by increasing temperatures even for higher density and the ion root is enhanced for higher density. Based on the usefulness of this approach to analyze E_r in LHD, calculations in a wide range have been performed to clarify the parameter region of interest where multiple solutions of E_r can exist. This is the region where E_r transition and bifurcation may be realized as already experimentally confirmed in CHS. The systematic calculations give a comprehensive understandings of experimentally observed E_r properties, which indicates an optimum path towards improved confinement.

KEYWORDS: radial electric field (E_r), ambipolar condition, neoclassical flux, electron root, multiple solutions of E_r, improved confinement

§1. Introduction

Recently, significant roles of radial electric field (E_r) in toroidal plasmas have been widely recognized to achieve improvemd confinement modes[1] such as H-mode[2] and internal transport barrier (ITB).[3] The potential pulsation has also been experimentally observed in CHS.[4] The abrupt change of E_r has been observed with a time scale much shorter than the energy confinement time scale between negative and positive states. This phenomenon is physically interpreted as the transition between two stable states of E_r with negative (ion root) and positive (electron root) values which can exist due to the nonlinear dependence of neoclassical transport fluxes on E_r. The electron thermal transport barrier has also been identified in CHS,[5] which contributes to the reduction of the density fluctuation associated with the structural variation of E_r profile. This gives the experimental evidence of the E_r domain interface as theoretically predicted.[6] The domain interface, across which different branches of the solution touch, appears in a medium which has multiple states.[7] The predicted parameter (density and temperatures) region for establishing E_r domain interface, where multiple solutions of E_r solutions can exist, is in semi-quantitatively good agreement with experimental results.[8] This also confirms the usefulness of the guidance to achieve an improved confinement by clarifying the parameter region of interest. The behaviour of this region is investigated for LHD[9] in this paper to promote experiments towards possible improved confinement. An analytical model for to calculations of the neoclassical particle fluxes is briefly explained in Sec. 2. In Sec. 3, an ambipolar E_r is examined for the parameters of some LHD discharges based on experimentally measured plasma profiles to compare calculated E_r with experimental ones. The qualitatively good agreement between these results validates this approach for the purpose to clarify the parameter region of interest where E_r domain interface may be realized. Finally, summary and discussions are given in Sec. 4.

§2. Model description

In this paper, neoclassical particle fluxes are calculated by the analytical formulae derived by Kovrizhnykh.[10] The E_r is determined with the ambipolar condition, $\Gamma_e = \Gamma_i$, where Γ_j denotes the particle flux of plasma species with $j = e$ for electrons and $j = i$ for ions. More precise calculations in realistic geometry are required to obtain more accurate fluxes such as by GNET code[11] which takes into account the fine structure of magnetic field and the contribution to particle fluxes from energetic particles. However, such computations are very time-consuming. The use of analytical formulae stimulates to clarify E_r properties in a wide range of temperature and density in a more transparent way.

Figure 1 shows the spectrum of the magnetic field in the Boozer coordinates[12] for two vacuum configurations with different position of the magnetic axis (R_{ax}), (a) $R_{ax} = 3.75$ m and (b) $R_{ax} = 3.60$ m. These equilibria are calculated with VMEC.[13] The curve with (0,0) denotes the difference of the uniform field strength from its value on the magnetic axis, $B_{0,0}(\rho) - B_{0,0}(0)$, and all other components are normalized by $B_{0,0}(0)$, where ρ is the normalized minor radius. For the case of $R_{ax} = 3.75$ m, the poloidal inhomogeneity of B ($|\epsilon_{1,0}|$) is almost equal to the geometrical inverse aspect ratio. On the other hand, for the case of $R_{ax} = 3.60$ m, it is about 2/3 times smaller than that of $R_{ax} = 3.75$ m with almost the same plasma minor radius. The contribution of satellite helicity, $\epsilon_{1,10}$, becomes larger for $R_{ax} = 3.60$ m even for inner region, although its edge value is almost equal to that of $R_{ax} = 3.75$ m. Another satellite helicity, $\epsilon_{3,10}$ also becomes apparent for $R_{ax} = 3.60$ m with the amplitude almost equal to that of $\epsilon_{1,10}$ at the plasma edge. Thus, the field structure of LHD in vacuum - low beta conditions for this range of R_{ax} can be approximately expressed as follows

$$B = B_0[1 + \epsilon_{1,0}\cos\theta + \epsilon_{2,10}\cos(2\theta - 10\zeta) + \epsilon_{1,10}\cos(\theta - 10\zeta) + \epsilon_{3,10}\cos(3\theta - 10\zeta)], \quad (2.1)$$

where (θ, ζ) are (poloidal, toroidal) angles, respectively.

In the original formulae by Kovrizhnykh, the poloidal inhomogeneity of B (denoted by δ in Ref.[10]) is simply defined by the geometrical inverse aspect ratio. This simple definition is no longer valid (cf., Fig. 1(b)). Thus, this δ is replaced by $|\epsilon_{1,0}|$. The helicity is defined there (denoted by $\hat{\epsilon}$) through the modified Bessel function based on the magnetic potential analysis,[14] which is also replaced by the effective helicity, ϵ_H. The convenient definition of ϵ_H is given in Ref.[15] This formula is applicable to the configuration control in LHD. The ϵ_H for Eq. (2.1) is defined by

$$\epsilon_H = (1/2\pi)\int_0^{2\pi} d\theta(\epsilon_{2,10}^2 + \epsilon_{1,10}^2 + \epsilon_{3,10}^2 + 2[\epsilon_{2,10}(\epsilon_{1,10} + \epsilon_{3,10})\cos\theta + \epsilon_{1,10}\epsilon_{3,10}\cos 2\theta])^{1/2}, \quad (2.2)$$

which is shown by solid curve in Figs. 1(a) and (b), respectively. The ϵ_H is enhanced in a plasma core region for $R_{ax} = 3.60$ m case due to the presence of a satellite helicity, $\epsilon_{1,10}$. The rotational transform is also given by VMEC calculations.

§3. Comparison with experimental results and the behaviour of parameter region of interest in LHD

In this section, firstly, the E_r calculated by the analytical formulae is compared with experimentally measured one. This is to check the relevance of the analytically estimated E_r in LHD and to make calculations in a wide range of parameters meaningful.

Some dependencies of E_r on plasma parameters have been identified in LHD such as "higher temperature (T) is required to realize electron root E_r ($E_r > 0$) for higher density (n)" and "E_r becomes negative for higher n (by gas-puffing and/or pellet injection) and becomes positive for lower n".[16] The latter tendency is firstly examined. During n scan experiments, n is varied with gas-puffing with keeping the value and profile of electron and ion temperatures (T_e and T_i) almost unchanged. Thus, calculations are performed by taking electron density (n_e) as a parameter using n and T profiles measured in this series of experiments ($R_{ax} = 3.75$ m and $B = 1.5$ T). The shape of n_e profile (hollow profile with the peak around $\rho \sim 0.8$, which has been the typical profile in LHD) is fixed to clearly see the dependence of E_r on n_e value itself. Figure 2 shows E_r solutions as a function of n_e on three flux surfaces, $\rho = 0.85$, 0.90 and 0.95. The experimentally measured E_r for $\rho > 0.85$ are also plotted for reference. The calculated E_r shows only one negative solution for $n_e \gtrsim 0.7 \times 10^{19} \equiv n_{e(c)}$ and solutions become multiple (three solutions) for $n_e \lesssim n_{e(c)}$. The middle one in these three solutions is unstable and one of other two solutions is considered to be realized. The $n_{e(c)}$ agrees with the observed threshold density for the transition from ion root to electron root. The maximum E_r values in electron root and ion root values are also well reproduced. This indicates that these calculations can qualitatively explain the tendency that "E_r becomes negative for higher n and becomes positive for lower n". It is noted that the difference of E_r values in the ion root for different flux surfaces is relatively smaller than that of electron root. This implies that the response of E_r on plasma parameters is more sensitive in electron root. It is also recognized that the maximum E_r (electron root) for each flux surface increases as ρ is increased for the same n_e. In the latter part of this section, the effect of ∇T_e on E_r is shown to be effective to realize electron root even for lower T_e. The ∇T_e increases towards the plasma edge associated with the edge pedestal formation.[17] This gives an enhanced (maximum) positive E_r at the outer radius even for lower T_e.

The measured E_r does not show the clear (or hard) transition from ion root to electron root as a function of n_e as shown in Fig. 2. This would be an influence of diffusivity on E_r associated with the particle orbit deviation from a flux surface.[18,19] Other possible mechanism is the influence of anomalous transport as is discussed in Ref.[20]

Figure 2 shows another interesting feature, that is, it seems that the electron root solution tends to be realized rather than ion root one for $n < n_{e(c)}$. This feature is different from the electron root observed in W7-AS, where the enhancement of ECH driven electron flux is required (ECH-driven electron root).[21,22] The ECH is also required for the enhancement of electron flux to re-

alize the electron root at the edge region in CHS.[23,24] On the other hand, electron root is realized even for NBI heated plasmas in LHD. One of reasons for this different feature may be smaller ion flux in LHD so that electron flux dominates to determine E_r.

The difference of $n_{e(c)}$ between cases of $R_{ax} = 3.75$ m and $R_{ax} = 3.60$ m is explained in Ref.[16] as the result of the difference of temperature ratio (T_e/T_i). One may consider that this difference can be explained in terms of magnetic configuration (different spectrum as in Fig. 1). However, this is less influential to vary $n_{e(c)}$ as explained below. Figure 3 shows calculated E_r solutions as a function of n_e for three cases: solutions for a reference data of temperatures $(T_e/T_i \sim 1.5)$ at $\rho = 0.9$ with $R_{ax} = 3.75$ m (broken curve), modified temperature values $(T_e/T_i = 1.0, T_e$ is decreased artificially) with temperature gradients being kept the same as reference ones (chain curve), and temperatures (values and profiles) are kept the same as reference ones but with magnetic field data of $R_{ax} = 3.60$ m (chain-dotted curve). The $n_{e(c)}$ does not vary between cases of $R_{ax} = 3.60$ m and 3.75 m with the same temperature values and gradients. On the other hand, it reduces for a case with $T_e/T_i = 1.0$ even for the case of $R_{ax} = 3.75$ m. The experimentally measured E_r are also shown in Fig. 3 for reference, which are thinned out from Figs. 1(a) and (b) in Ref.[16] The black circles are the results for the case of $R_{ax} = 3.75$ m with $T_e/T_i \sim 1.5$ and open ones for $R_{ax} = 3.60$ m with $T_e/T_i \sim 1.0$. The experimentally obtained $n_{e(c)}$ is rather well reproduced by calculations depending on the temperature ratio regardless of the difference of R_{ax}, which verifies the statement in Ref.[16] The results for neoclassical calculation shown in Fig. 1(b) in Ref.[16] ($R_{ax} = 3.60$ m) are obtained with $T_e/T_i \sim 1$ with almost same gradients as those of reference ones. If one perform calculations with temperature profiles with $T_e/T_i > 1$, $n_{e(c)}$ becomes larger.

Now, the dependence of E_r on temperature value is investigated to consider the tendency that "higher T is required to realize electron root for higher n". This can be expressed in other words as "electron root is possible even for higher n_e when temperatures are increased". Calculations are performed in a wide range of temperature space, (T_i, T_e) taking n_e as a parameter to check this tendency. Temperatures are amplified with keeping profiles to explore temperature region up to 3 keV (at $\rho = 0.9$) both for T_i and T_e. Figure 4(a) shows the dependence of the region of interest (surrounded region) on n_e. The E_r is singly negative below the lower boundary and singly positive beyond the upper boundary. The original value of n_e is about 0.75×10^{19} m^{-3}, which is multiplied with the amplification parameter (*namp*) as listed in the figure ($namp = 0.5, 1, 2, 5$) with keeping its profile unchanged. Of course, the ion density (n_i) is also amplified with the same *namp* for each case. It is seen that higher T (especially T_e) are required to reach the region of interest and to realize electron root for higher n. This indicates that E_r tends to become positive as n is decreased with keeping temperatures. For example, for $T_i = T_e = 1.5$ keV, E_r is negative for $namp = 5$ case, positive for $namp = 0.5$ case and multiple solutions exist for $namp = 1$ and 2 cases. This result well describes the experimentally observed tendency that "higher T is required to realize electron root for higher n". It can also demonstrate that E_r shows transition from negative to positive as n_e is decreased for fixed temperatures, which coincide with the tendency that "E_r becomes negative for higher n and becomes positive for lower n". The density scan calculations for Figs. 2 and 3 are regarded as a slice cut of this diagram (Fig. 4(a)) for fixed temperatures. Thus, this diagram is valuable to make out general tendency of E_r behavior on the wide range of (T_i, T_e) space with density dependence.

To understand this response of the parameter region of interest for the variation of n, following simplified expressions for particle fluxes are examied, which have been utilized to investigate width of the region of interest in (n, T_e) space in Ref.[8]

$$\begin{aligned} \Gamma_e &\sim \frac{n}{a} D_e (N - X + \beta_1 Y_e), \\ \Gamma_i &\sim \frac{n}{a} D_i \frac{1}{1 + C_i X^2} (N + \eta X + \beta_2 Y_i), \end{aligned} \tag{3.1}$$

where a is the plasma minor radius, $X = eaE_r/T_e$, $N = -an'/n$, $Y_j = aT_j'/T_j$, $C_j = 1.5(B_{1,0}/\epsilon_H)^{1/2}(T_e/\nu_j r B e a)^2$, $D_j = B_{1,0}^2 \epsilon_H^{1/2} v_{D_j}/\nu_j$ and $\eta = T_e/T_i$. Here, the prime denotes the derivative with respect to r and v_{D_j} is the drift velocity and β_1 and β_2 are numerical constants both close to 3.5.[25] The term $C_e X^2$ in the denominator of Γ_e is neglected because of its weaker contribution than that in ion flux ($C_i X^2$ term). The denominator of Γ_i causes the nonlinear dependence of Γ_i on E_r, and on the other hand, electron flux depends on E_r linearly. The intersections of these two fluxes are ambipolar E_r solutions which we have focused in this paper. This situation is schematically shown in Fig. 4 in Ref.,[8] where five cases (from (i) to (v)) are shown according to the level of Γ_e. The ion (electron) root region in temperature space (cf., below the lower (above the upper) boundary in Fig. 4(a)) corresponds to a situation where $\Gamma_e = \Gamma_i$ is realized only for $X < 0 (X > 0)$, which is shown by case (v) ((i)), respectively. The region of interest corresponds to situations shown from (ii) to (iv) where three intersections are possible. The analytic calculation with $Y_e = Y_i = 0$ (for simplicity) to have degenerating solutions for X leads to the relation for T_e on boundary of the region of interest, $T_{e(b)}$ (both for upper and lower boundary), as $T_{e(b)} \propto n^{0.4}$, which arises from the C_i term ($\propto n^{-2}$) in Γ_i. This well explaines the shift of the region of interest towards higher T_e region shown in Fig. 4(a). It is understood physically as follows. The

effect of $\boldsymbol{E} \times \boldsymbol{B}$ drift to reduce Γ_i is weakened for higher n case with higher collisionality, which weakens the reduction of Γ_i with X so that higher T_e requires to revive $\Gamma_e = \Gamma_i$ by enhancing Γ_e.

This diagram is now re-considered in terms of the electron collision frequency, ν_e^*, and temperature ratio, T_e/T_i, as in Fig. 4(b). The ν_e^* is normalized by the collision frequency corresponding to the boundary between banana and plateau regime. The surrounded region corresponds to the region of interest. It indicates that the parameter region of interest appears when ν_e^* locates deep inside of $1/\nu$ regime and the critical ν_e^* for entering to the region of interest, $\nu_{e(c)}^*$, is about 0.2 for all cases of *namp* in this case. Figure 4(b) gives the clear information of the dependence of the region of interest on ν_e^* and T_e/T_i, on the other hand, Fig. 4(a) is useful to consider concretely how to realize $\nu_{e(c)}^* \sim 0.2$ with the combination of temperatures and density. Figure 4(b) shows another interesting fact. Only the electron root is realized in a wide range of ν_e^* when $T_e/T_i \gtrsim 3.5$, which coincides with the estimate in Ref. [20]

As described above, E_r determined based on extended analytical formulae can be regarded to explain qualitative dependence of E_r observed in LHD on plasma parameters such as temperatures and density. This qualitative agreement with experimental observations really encourages the present approach to examine transition and bifurcation properties of E_r towards improved confinement in LHD.

The dependence of the region of interest on several parameters in addition to n is examined at $\rho = 0.9$ using the experimental data. These calculations are valuable to study individual parameter dependence.

Figure 5(a) shows the dependence on the magnetic field strength, B, for $namp = 1$ case. As B is increased, the region of interest shifts towards higher T (especially T_e) region. When B is increased, Γ_i increases due to the term C_i (Eq. (3.1)), which gives $T_{e(b)} \propto B^{0.4}$. It implies that higher B reduces $\boldsymbol{E} \times \boldsymbol{B}$ drift velocity with E_r being fixed, which weakens the reduction of Γ_i due to E_r so that higher T_e is required to revive $\Gamma_e = \Gamma_i$ by enhancing Γ_e. Thus, the boundary of the region of interest shifts towards higher T_e region as shown in Fig. 5(a). It is recognized that $T_{e(b)}$ for the case of $B = 2.5$ T is about $1.6 = (2.5/0.75)^{0.4}$ times higher than that for $B = 0.75$ T case for a fixed temperature ratio as anticipated with $T_{e(b)} \propto B^{0.4}$. Figure 5(a) is also re-plotted in terms of ν_e^* and T_e/T_i in Fig. 5(b). It is clearly recognized that $\nu_{e(c)}^*$ becomes smaller ($T_e(b)$ becomes higher) as B is increased due to the weaker reduction of Γ_i due to E_r as explained above.

Effects of ∇T_e, ∇T_i and $\nabla n_e(n_i)$ are also examined associated with the edge pedestal formation. The gradients are amplified with parameters, *tegamp* for T_e, *tigamp* for T_i and *ngamp* for $n_{e,i}$, respectively. As shown in Fig. 6(a), the variation of ∇T_i makes little difference even when its gradient is doubled ($(tegamp, tigamp) = (1, 2)$ case), while doubling ∇T_e is effective to shift the region of interest to lower T_e region ($(tegamp, tigamp) = (2, 1)$ case). Based on Eq. (3.1) with finite Y_js and $N = 0$, the following condition is obtained to satisfy $\Gamma_e = \Gamma_i$ as

$$X^3 + AX^2 + BX + C = 0, \qquad (3.2)$$

where $A \equiv -\beta_1 Y_e$, $B \equiv (1 + D_i/D_e\eta)/C_i$ and $C \equiv \frac{Y_i}{C_i}(\beta_2 \frac{D_i}{D_e} - \beta_1 \frac{Y_e}{Y_i})$. It is noted that $D_i/D_e = (m_i/m_e)^{1/2}(T_i/T_e)^{7/2}$ with $m_i(m_e)$ being mass of ion (electron). Since $D_i/D_e \sim 15$ for this case with $T_i/T_e \sim 0.75$ and $Y_e/Y_i \sim 1.6$, the second term in bracket in C can be neglected compared to the first term. It is recognized that the variation of Y_e (representing ∇T_e) affects the nonlineality of Eq. (3.2) through A. The Γ_e is enhanced when Y_e is increased (cf., Eq. (3.1)), which makes it possible to reach electron root even at lower T_e region. On the other hand, the increase of Y_i tends to eliminate electron root solution by shifting cubic curve (left hand side of Eq. (3.2)) through the increase of C. The higher T_e is required to revive electron root by enhancing Γ_e, which is seen in Fig. 6(a). Figure 6(b) shows that the region of interest is less influenced by *ngamp*, which implies that E_r is mainly attributed to the temperature gradient. The effect of the denisty gradient may be more easily examined at a location with less temperature gradient.

The results described in this section have shown that the parameter region of interest is shifted to a lower T (especially T_e) region by reducing B and increasing ∇T_e for lower n. This situation can be experimentally tested in a controlled manner at the edge region in LHD where the pedestal-type temperature gradient is formed[17] with lower n. It is interesting to examine how electron root behaves at the plasma edge associated with the edge pedestal and how it affects the plasma confinement property.

Electron root E_r can be enhanced for some radial portion of plasma and it is also anticipated to have a large E_r shear around E_r domain interface if there is only one ion root solution at neighboring flux surface. Thus, the analysis at the different radius should also be performed to examine the possibility of E_r domain interface. The computationally clarified dependence of the parameter region of interest on plasma parameters examined in this paper gives the basis for this further study.

§4. Summary and Discussions

The E_r properties have been examined for LHD to indicate the guidance towards improved confinement associated with E_r transition and bifurcation. The E_r is obtained based on the ambipolar condition with the neoclassical flux calculated by the analytical formulae. This approach is appropriate for the purpose of this paper to

clarify E_r properties in a wide range of temperature and density in a more tranceparent way. The original model magnetic field in Ref. [10] is extended to include sideband helicities to be applicable to the configuration control in LHD. Some of other equilibrium parameters are directly given from three dimensional equilibrium calculations based on experimentally measured plasma profiles.

The calculated E_r is compared with experimentally measured E_r to check the validity of this approach for LHD and to make wide range calculations meaningful. The experimentally observed tendency that E_r becomes positive as n is decreased is qualitatively well reproduced. The threshold density for the transition from ion root to electron root is also reproduced based on calculations, which is again in qualitatively good agreement with experimental results.

Based on this assurance of this approach for LHD, wide range calculations have been performed to clarify the parameter region of interest. This is the region where E_r transition and bifurcation is possible as already experimentally confirmed in CHS. As n is increased, this region shifts towards higher T (especially T_e) region, which is consistent with above mentioned experimental result for the transition from ion root to electron root below the threshold density. This tendency clarified with calculations has also been experimentally confirmed based on the following two experimental results. One is that the positive E_r is observed by increasing temperatures even for higher n. Another is that the negative E_r is enhanced for higher n. The dependence of the region of interest on other plasma parameters are also examined such as B and gradients of temperatures and density. This systematic calculation can give comprehensive understandings of experimentally observed tendencies of E_r properties, which can give the appropriate guidance towards improved confinement. In this paper, E_r properties are examined at a certain radius for a particular discharge as an example. The analysis for different radius should also be performed to examine the possibility of E_r domain interface formation. Further detailed experimental test of this guidance will appear in a separate paper.

Acknowledgements

This work has been supported by grant-in-aid from the Ministry of Education, Culture, Sports, Science and Technology, Japan.

1) K.Itoh and S.-I.Itoh, Plasma Phys. Control. Fusion **38**(1996)1.
2) F.Wagner et al., Phys. Rev. Lett. **49**(1982)1408.
3) T.Fujita, et al , Phys. Rev. Lett. **78**(1997)2377.
4) A.Fujisawa et al., Phys. Rev. Lett. **79**(1997)1054.
5) A.Fujisawa et al., Phys. Rev. Lett. **82**(1999)2669, A.Fujisawa et al., Phys. Plasmas **7**(2000)4152.
6) K. Itoh, H. Sanuki, S.-I. Itoh, A.Fukuyama, A. Fujisawa, M. Yagi, K. Ida J. Plasma Fusion Res. Suppl. **74**(1998)282 (in Japanese).
7) K.Itoh, S.-I.Itoh and A.Fukuyama, *Transport and Structural Formation in Plasmas*, Institute of Physics Publishing, Bristol and Philadelphia, (1999).
8) H.Sanuki, K.Itoh, M.Yokoyama et al , J Phys Soc. Jpn **69**(2000)445
9) A.Iyoshi et al., Nucl. Fusion **39**(1999)1245.
10) L.M.Kovrizhnykh, Nucl. Fusion **24**(1984)435.
11) S. Murakami et al., Nucl. Fusion **40**(2000)693.
12) A.H.Boozer, Phys. Fluids, **23**(1980)904.
13) S.P.Hirshman, et al., Comput. Phys. Commun. **43**(1986)143.
14) A.I.Morozov and L.S.Solov'ev, Reviews of Plasma Physics Vol.2, p.1 (ed. M.A.Leontovich) Consultants Bureau, New York (1966).
15) K.C.Shaing and S.A.Hokin, Phys. Fluids **26**(1983)2136.
16) K.Ida et al., IAEA-CN-77/EX9/4 presented at 18th IAEA Fusion Energy Conf., Sorrento, Italy (2000).
17) N.Ohyabu, A.Fujisawa et al., Phys. Plasmas **7**(2000)1802.
18) K.C.Shaing, Phys. Fluids, **27**(1984)1567.
19) H.Sanuki, K.Itoh, J.Todoroki et al., Phys. Scripta **52**(1995)461.
20) K.Itoh et al , submitted to J. Phys. Soc. Japan (2000).
21) H.Maaβberg et al., Phys. Plasmas **7**(2000)295.
22) S.Murakami et al., Nucl. Fusion **40**(2000)693.
23) H.Idei et al., Phys. Rev. Lett. **71**(1993)2220.
24) S.Murakami et al., in Proc. 17th IAEA Fusion Energy Conf., (Montreal, 1996), Vol.2, IAEA, Vienna (1997)157. S.Murakami et al., Plasma Phys. Rep. **23**(1997)556.
25) J.W.Conner and R.J.Hastie, Phys. Fluids, **17**(1974)114.

Fig. 1. Fourier spectrum of B, $\epsilon_{m,n}$, in the Boozer coordinates for vacuum configurations in LHD with R_{ax} = (a) 3.75 m and (b) 3.60 m. The effective helicity, ϵ_H, is also shown by solid curve for reference.

Fig. 2. Calculated E_r at $\rho = 0.85$, 0.9 and 0.95 by varying only the density as a parameter using the density and temparature profiles observed in the density scan experiments. The experimentally measured E_r for $\rho > 0.85$ are also plotted for reference.

Fig. 3. Calculated E_r as a function of n_e for three cases: solutions for a reference data of temparatures ($T_e/T_i \sim 1.5$) at $\rho = 0.9$ with R_{ax} = 3.75 m (broken curve), modified temperature values ($T_e/T_i = 1.0$, T_e is decreased artificially) with temperature gradients being kept as same as those of reference ones (chain curve), and temperatures (values and profiles) are kept the same as those of reference ones but with magnetic field data of R_{ax} = 3.60 m (chain-dotted curve).

Fig. 4. (a) Dependence of the parameter region of interest on n parameterized by $namp$ ($namp = 0.5, 1, 2, 5$) in the (T_i, T_e) plane. (b) Figure 4(a) is re-plotted in terms of the normalized electron collision frequency, ν_e^*, and T_e/T_i.

Fig. 5. Dependence of the parameter region of interest on (a) B (B = 0.75 T, 1.5 T, 2.5 T) in the (T_i, T_e) plane. (b) Figure 5(a) is re-plotted in terms of ν_e^*, and T_e/T_i.

Fig. 6. Dependence of the parameter region of interest on (a) the temperature gradient parameterized by $(tegamp, tigamp)$ for amplification factor for (T_e, T_i), respectively : $((tegamp, tigamp) = (1,1), (1,2)$ and $(2,1))$ and (b) the density gradient parameterized by $ngamp$ for amplification factor for n ($ngamp = 0.5, 1, 2$).

Fig. 1 (a)

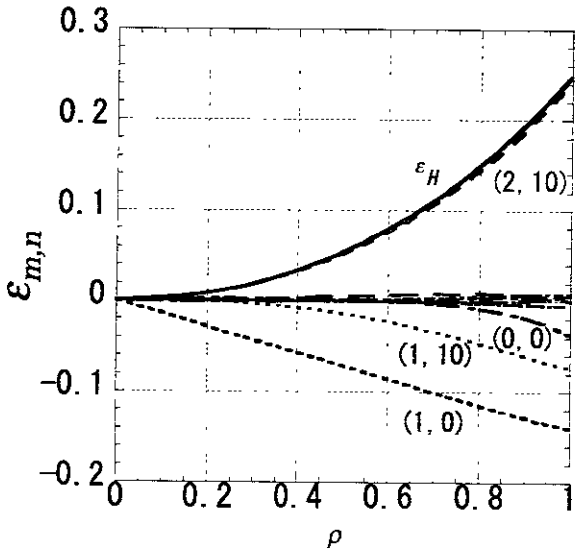

Fig. 1 (b)

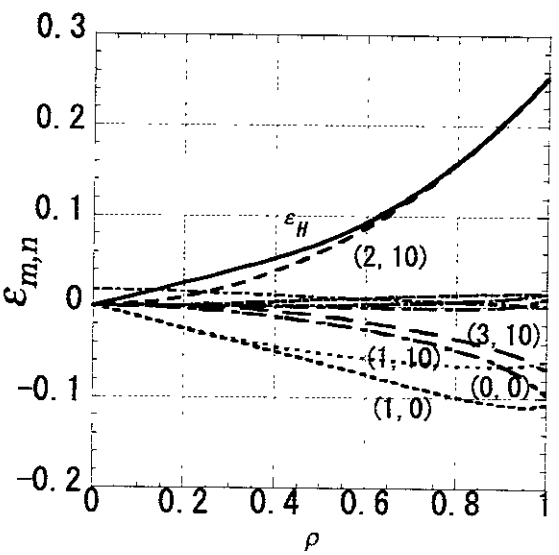

Fig. 2

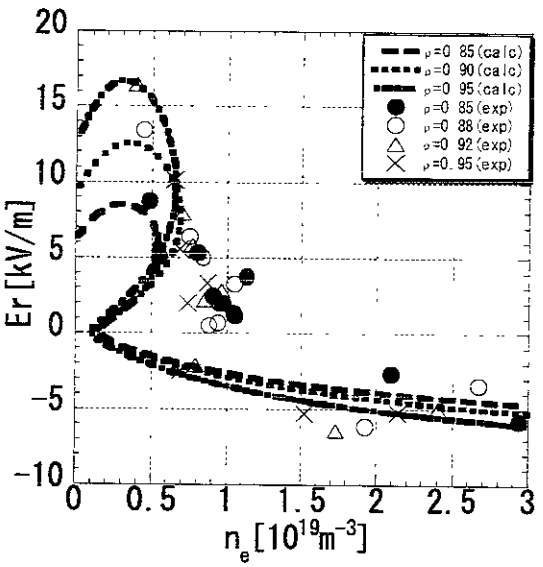

Fig. 3

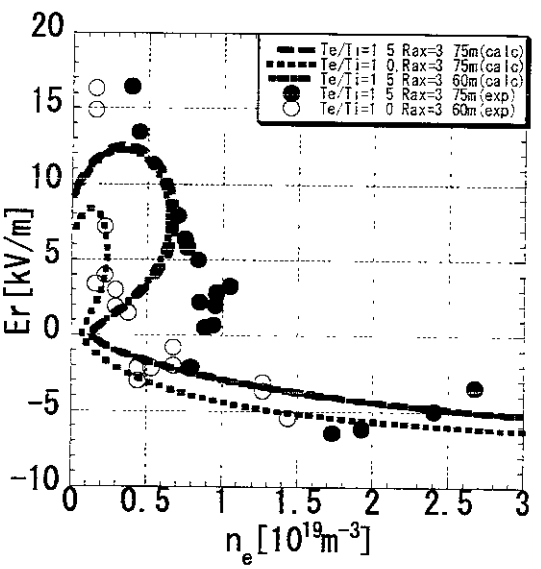

Fig. 4(a)

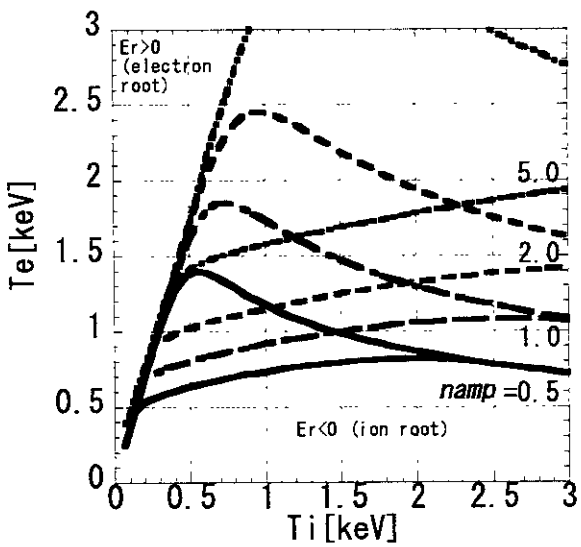

Fig. 4(b)

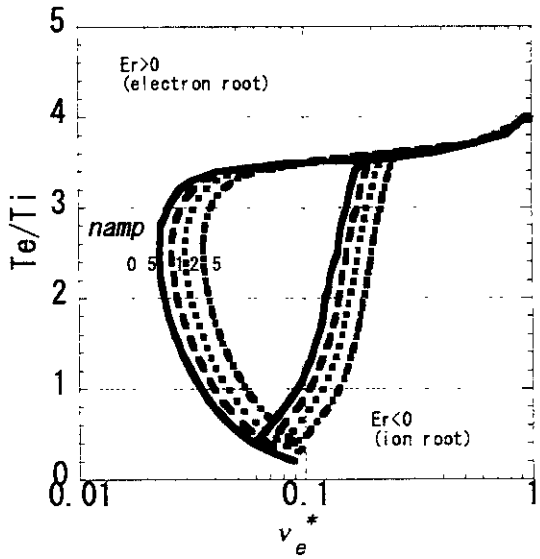

Fig. 5(a)

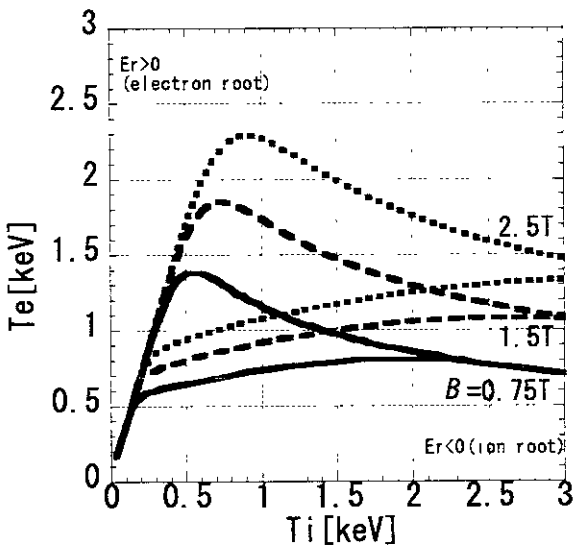

Fig. 5(b)

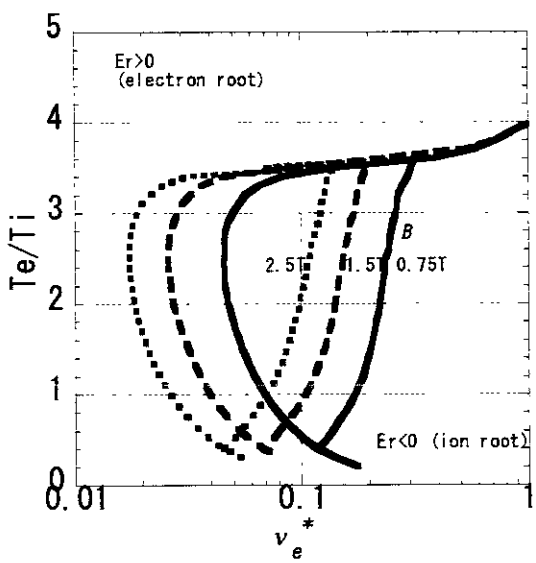

Fig. 6(a)

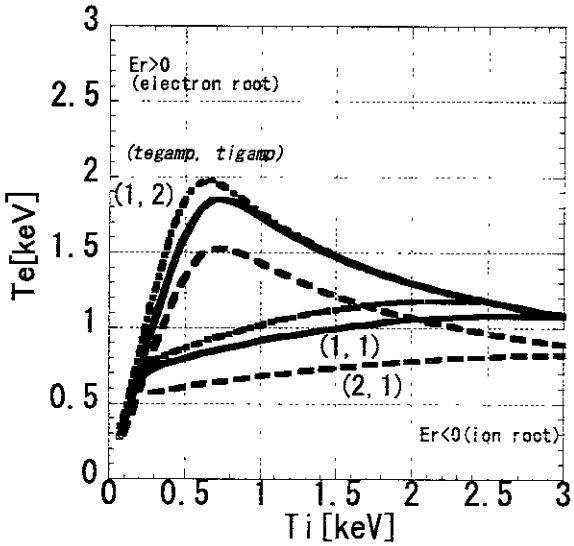
Er>0
(electron root)
(tegamp, tigamp)
(1, 2)
(1, 1)
(2, 1)
Er<0(ion root)
Te[keV]
Ti[keV]
0
0.5
1
1.5
2
2.5
3

Fig. 6(b)

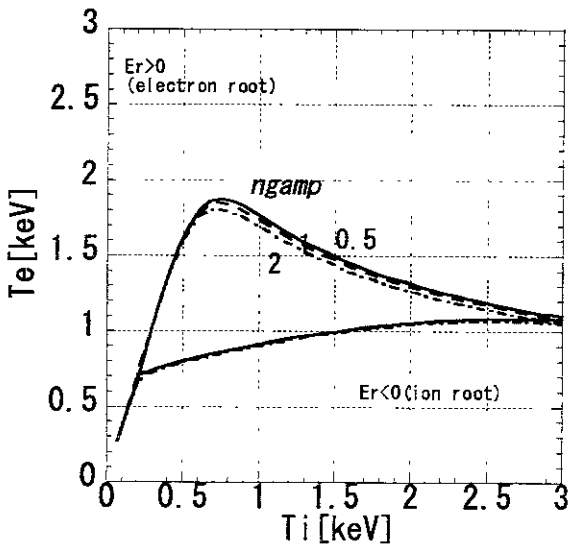
Er>0
(electron root)
ngamp
0.5
1
2
Er<0(ion root)
Te[keV]
Ti[keV]
0
0.5
1
1.5
2
2.5
3

Recent Issues of NIFS Series

NIFS-670 L. Hadzievski, M M Skoric and T. Sato
On Origin and Dynamics of the Discrete NLS Equation Nov 2000

NIFS-671 K Ohkubo, S Kubo, H Idei, I Shimozuma, Y Yoshimura, J Leuterer, M Sato and Y Takita,
Analysis of Oversized Sliding Waveguide by Mode Matching and Multi-Mode Network Theory Dec 2000

NIFS-672 C Das, S Kida and S Goto,
Overall Self-Similar Decay of Two-Dimensional Turbulence Dec 2000

NIFS-673 L A Bureyeva, T Kato, V S Lisitsa and C Namba
Quasiclassical Representation of Autoionization Decay Rates in Parabolic Coordinates Dec 2000

NIFS-674 L A Bureyeva, V S Lisitsa and C Namba,
Radiative Cascade Due to Dielectronic Recombination Dec 2000

NIFS-675 M F Heyn, S V Kasilof W Kernbichler, K Matsuoka, V V Nemov, S Okamura O S Pavlichenko,
Configurational Effects on Low Collision Plasma Confinement in CHS Heliotron/Torsatron, Jan 2001

NIFS-676 K Itoh,
A Prospect at 11th International Toki Conference - Plasma physics, quo vadis?, Jan 2001

NIFS-677 S Satake, H Sugama, M Okamoto and M Wakatani,
Classification of Particle Orbits near the Magnetic Axis in a Tokamak by Using Constants of Motion, Jan 2001

NIFS-678 M Tanaka and A Yu Grosberg
Giant Charge Inversion of a Macroion Due to Multivalent Counterions and Monovalent Coions Molecular Dynamics Studyn, Jan 2001

NIFS-679 K Akaishi, M Nakasuga, H Suzuki, M Iima, N Suzuki, A Komori, O Motojima and Vacuum Engineering Group,
Simulation by a Diffusion Model for the Variation of Hydrogen Pressure with Time between Hydrogen Discharge Shots in LHD, Feb 2001

NIFS-680 A Yoshizawa, N Yokoi, S Nisizima, S -I Itoh and K Itoh
Variational Approach to a Turbulent Swirling Pipe Flow with the Aid of Helicity, Feb 2001

NIFS-681 Alexander A Shishkin
Estafette of Drift Resonances, Stochasticity and Control of Particle Motion in a Toroidal Magnetic Trap, Feb 2001

NIFS-682 H Momota and G H Miley,
Virtual Cathode in a Spherical Inertial Electrostatic Confinement Device, Feb 2001

NIFS-683 K Saito, R Kumazawa, T Mutoh, T Seki, T Watari, Y Torii, D A Hartmann, Y Zhao, A Fukuyama, F Shimpo G Nomura, M Yokota, M. Sasao, M Isobe, M Osakabe, T Ozaki, K Narihara, Y Nagayama, S Inagaki, K Itoh, S Morita, A V Krasilnikov, K Ohkubo, M Sato, S Kubo, T Shimozuma, H Idei, Y Yoshimura, O Kaneko, Y Takeiri, Y Oka, K Tsumori, K Ikeda, A Komori, H Yamada, H Funaba, K Y Watanabe, S. Sakakibara, M. Shoji, R Sakamoto, J. Miyazawa, K Tanaka, B J Peterson, N Ashikawa, S Murakami, T Minami, S. Ohakachi, S Yamamoto, S Kado, H Sasao, H Suzuki, K Kawahata, P deVries, M. Emoto, H Nakanishi, T Kobuchi, N Inoue, N Ohyabu, Y Nakamura, S Masuzaki, S Muto, K Sato, T Morisaki, M Yokoyama, T Watanabe, M Goto, I. Yamada, K Ida T Tokuzawa, , N Noda, S Yamaguchi K Akaishi, A Sagara, K Toi K Nishimura, K Yamazaki, S Sudo Y Hamada, O Motojima, M Fujiwara,
Ion and Electron Heating in ICRF Heating Experiments on LHD, Mar 2001

NIFS-684 S Kida and S Goto,
Line Statistics Stretching Rate of Passive Lines in Turbulence Mar 2001

NIFS-685 R Tanaka, T Nakamura and T Yabe,
Exactly Conservative Semi-Lagrangian Scheme (CIP-CSL) in One-Dimension Mar 2001

NIFS-686 S Toda and K Itoh,
Analysis of Structure and Transition of Radial Electric Field in Helical Systems Mar 2001

NIFS-687 T Kuroda and H Sugama,
Effects of Multiple-Helicity Fields on Ion Temperature Gradient Modes Apr 2001

NIFS-688 M Tanaka,
The Origins of Elctrical Resistivity in Magnetic Reconnection Studies by 2D and 3D Macro Particle Simulations Apr 2001

NIFS-689 A Maluckov, N Nakajima, M Okamoto, S Murakami and R Kanno,
Statistical Properties of the Neoclassical Radial Diffusion in a Tokamak Equilibrium Apr 2001

NIFS-690 Y Matsumoto, T Nagaura, Y Itoh, S-I Oikawa and T Watanabe,
LHD Type Proton-Boron Reactor and the Control of its Peripheral Potential Structure, Apr 2001

NIFS-691 A Yoshizawa, S.-I Itoh, K. Itoh and N Yokoi,
Turbulence Theories and Modelling of Fluids and Plasmas Apr 2001

NIFS-692 K Ichiguchi, T Nishimura, N Nakajima, M Okamoto, S -i. Oikawa, M Itagaki,
Effects of Net Toroidal Current Profile on Mercier Criterion in Heliotron Plasma Apr 2001

NIFS-693 W Pei, R Horiuchi and T Sato,
Long Time Scale Evolution of Collisionless Driven Reconnection in a Two-Dimensional Open System, Apr 2001

NIFS-694 L N Vyacheslavov, K. Tanaka, K Kawahata,
CO2 Laser Diagnostics for Measurements of the Plasma Density Profile and Plasma Density Fluctuations on LHD Apr 2001

NIFS-695 T Ohkawa,
Spin Dependent Transport in Magnetically Confined Plasma May 2001

NIFS-696 M Yokoyama, K Ida, H Sanuki, K Itoh, K Narihara, K Tanaka, K Kawahata, N Ohyabu and LHD experimental group
Analysis of Radial Electric Field in LHD towards Improved Confinement, May 2001